Supplementary Material to: Optimisation of romosozumab plus denosumab sequential treatments against postmenopausal osteoporosis. Insights from in silico simulations

Rocío Ruiz-Lozano[a,1], José Luis Calvo-Gallego[a,1,*], Peter Pivonka[b,1], Javier Martínez-Reina[a,1]

[a] *Departmento de Ingeniería Mecánica y Fabricación, Universidad de Sevilla, Seville 41092, Spain*
[b] *School of Mechanical, Medical and Process Engineering, Queensland University of Technology, QLD 4000, Australia*
[c] *Garvan Institute of Medical Research, Sydney, Australia*

1. Introduction

In this document we provide those details of the mathematical model not provided in the main document. More precisely, we explain here those features of the original model by Martin et al. [1] which remained unchanged; while those that have been modified or are more relevant to the study are presented in the main document.

This document is structured as follows: In section 2 we present the general equations for competitive binding between ligands and receptors; the specific equations for the competitive binding of the complex RANK-RANKL-OPG and Wnt–Scl–LRP5/6 are given in sections 3 and 4 respectively. The co-regulation of RANKL levels via the antagonistic effect of PTH and nitric oxide is presented in section 5. The equations related to microestructural damage are shown in section 6 and the upregulation of RANKL expressed by osteocytes due to damage is given in section 7. The equations of the PK model of Denosumab are given in section 8. The equations related to the regulatory effect of TGF-β are given in section 9. Section 10 describes the term of proliferation of osteoblast precursors. The algorithm of bone

*Corresponding author

mineralisation is shown in section 11. Finally, the model constants are given in Table 1.

2. Competitive binding

Many biological processes are controlled by binding of biochemical factors which act as receptor and ligand. In some of them two or more ligands compete to bind to the receptor. This is the case of Wnt and sclerostin that compete to bind to LRP5/6 to control the proliferation of osteoblast precursors and also the case of RANK, OPG and Dmab which compete to bind to RANKL to control the differentiation of osteoclast precursors into mature active osteoclasts.

Let us consider separately the binding of a given receptor R to its ligands A and B to form, respectively, the complexes A–R and B–R. Let us consider for each species X=A,B,R a production term P_X and a degradation term D_X, along with a degradation term for the complex D_{X-Y}. Let K^r_{X-Y} and K^f_{X-Y} be the reverse and forward binding reaction constants, respectively.

$$\begin{array}{ccccccc} \downarrow P_R & & \downarrow P_A & & & & \\ R & + & A & \overset{K^f_{A-R}}{\underset{K^r_{A-R}}{\rightleftharpoons}} & A-R & \overset{D_{A-R}}{\rightharpoonup} & \emptyset \\ \downarrow D_R & & \downarrow D_A & & & & \end{array} \tag{1}$$

$$\begin{array}{ccccccc} \downarrow P_R & & \downarrow P_B & & & & \\ R & + & B & \overset{K^f_{B-R}}{\underset{K^r_{B-R}}{\rightleftharpoons}} & B-R & \overset{D_{B-R}}{\rightharpoonup} & \emptyset \\ \downarrow D_R & & \downarrow D_B & & & & \end{array} \tag{2}$$

The law of mass action provides the following set of differential equations:

$$\frac{d\,[A-R]}{dt} = K^f_{A-R}\,[A]\,[R] - K^r_{A-R}\,[A-R] - \tilde{D}_{A-R}\,[A-R] \tag{3a}$$

$$\frac{d\,[B-R]}{dt} = K^f_{B-R}\,[B]\,[R] - K^r_{B-R}\,[B-R] - \tilde{D}_{B-R}\,[B-R] \tag{3b}$$

$$\frac{d\,[A]}{dt} = P_A - \tilde{D}_A\,[A] + K^r_{A-R}\,[A-R] - K^f_{A-R}\,[A]\,[R] \tag{3c}$$

$$\frac{\mathrm{d}\,[\mathrm{B}]}{\mathrm{dt}} = \mathrm{P_B} - \tilde{\mathrm{D}}_\mathrm{B}\,[\mathrm{B}] + \mathrm{K}^\mathrm{r}_{\mathrm{B-R}}\,[\mathrm{B-R}] - \mathrm{K}^\mathrm{f}_{\mathrm{B-R}}\,[\mathrm{B}]\,[\mathrm{R}] \tag{3d}$$

$$\begin{aligned}\frac{\mathrm{d}\,[\mathrm{R}]}{\mathrm{dt}} =& \mathrm{P_R} - \tilde{\mathrm{D}}_\mathrm{R}\,[\mathrm{R}] + \mathrm{K}^\mathrm{r}_{\mathrm{A-R}}\,[\mathrm{A-R}] + \mathrm{K}^\mathrm{r}_{\mathrm{B-R}}\,[\mathrm{B-R}] \\ &- \mathrm{K}^\mathrm{f}_{\mathrm{A-R}}\,[\mathrm{A}]\,[\mathrm{R}] - \mathrm{K}^\mathrm{f}_{\mathrm{B-R}}\,[\mathrm{B}]\,[\mathrm{R}]\end{aligned} \tag{3e}$$

where $[\mathrm{X}]$ and $[\mathrm{X-Y}]$ represent, respectively, the concentration of species X and complex X-Y. The degradation terms are assumed proportional to the concentration of the species, i.e. $\mathrm{D_X} = \tilde{\mathrm{D}}_\mathrm{X}\,[\mathrm{X}]$, with $\tilde{\mathrm{D}}_\mathrm{X}$ being the degradation rate.

Following Pivonka et al. [2] we assume that the binding reactions are much faster than the cell responses they produce and hence a quasi-steady state can be assumed, implying that the time derivatives of Eqs. (3) are null. This condition in Eqs. (3a) and (3b) yield:

$$[\mathrm{A-R}] = \frac{[\mathrm{A}]\,[\mathrm{R}]}{\mathrm{K_{A-R}}} \tag{4a}$$

$$[\mathrm{B-R}] = \frac{[\mathrm{B}]\,[\mathrm{R}]}{\mathrm{K_{B-R}}} \tag{4b}$$

where:

$$\mathrm{K_{A-R}} = \frac{\mathrm{K}^\mathrm{r}_{\mathrm{A-R}} + \tilde{\mathrm{D}}_{\mathrm{A-R}}}{\mathrm{K}^\mathrm{f}_{\mathrm{A-R}}} \tag{5a}$$

$$\mathrm{K_{B-R}} = \frac{\mathrm{K}^\mathrm{r}_{\mathrm{B-R}} + \tilde{\mathrm{D}}_{\mathrm{B-R}}}{\mathrm{K}^\mathrm{f}_{\mathrm{B-R}}} \tag{5b}$$

The stationarity condition of Eqs. (3c)-(3e) yields:

$$[\mathrm{A}] = \frac{\mathrm{P_A}}{\tilde{\mathrm{D}}_\mathrm{A} + \frac{\tilde{\mathrm{D}}_{\mathrm{A-R}}}{\mathrm{K_{A-R}}}\,[\mathrm{R}]} \tag{6a}$$

$$[\mathrm{B}] = \frac{\mathrm{P_B}}{\tilde{\mathrm{D}}_\mathrm{B} + \frac{\tilde{\mathrm{D}}_{\mathrm{B-R}}}{\mathrm{K_{B-R}}}\,[\mathrm{R}]} \tag{6b}$$

$$[\mathrm{R}] = \frac{\mathrm{P_R}}{\tilde{\mathrm{D}}_\mathrm{R} + \frac{\tilde{\mathrm{D}}_{\mathrm{A-R}}}{\mathrm{K_{A-R}}}\,[\mathrm{A}] + \frac{\tilde{\mathrm{D}}_{\mathrm{B-R}}}{\mathrm{K_{B-R}}}\,[\mathrm{B}]} \tag{6c}$$

If the degradation ($\tilde{\mathrm{D}}_{\mathrm{X}}$,$\tilde{\mathrm{D}}_{\mathrm{X-Y}}$), production ($\mathrm{P_X}$) and dissociation constants, ($\mathrm{K_{X-Y}}$) are known, (6) constitutes a non-linear system of three equations with three unknowns, namely [A], [B], [R].

The total concentration of a receptor is the sum of the concentrations of the receptor which is found free and bound to ligands, i.e.:

$$[\mathrm{R}]_{\mathrm{tot}} = [\mathrm{R}] + [\mathrm{A-R}] + [\mathrm{B-R}] = [\mathrm{R}] \left(1 + \frac{[\mathrm{A}]}{\mathrm{K_{A-R}}} + \frac{[\mathrm{B}]}{\mathrm{K_{B-R}}}\right) \tag{7}$$

where Eqs. (4) have been used. The stationarity condition is equivalent to establish that the production rate of a species must equal the degradation rate, including all its forms, free and bound. For instance, in the case of the receptor that can bind to different ligands, this condition reads:

$$\mathrm{P_R} = \tilde{\mathrm{D}}_{\mathrm{R}}\,[\mathrm{R}] + \sum_{\mathrm{L}} \tilde{\mathrm{D}}_{\mathrm{L-R}}\,[\mathrm{L-R}] \tag{8}$$

which can be obtained from Eqs. (3a), (3b) and (3e) by imposing that the stationarity condition is met, ($\frac{\mathrm{d}\,[\mathrm{R}]}{\mathrm{dt}} = \frac{\mathrm{d}\,[\mathrm{L-R}]}{\mathrm{dt}} = 0 \quad \forall\, \mathrm{L} = \mathrm{A}, \mathrm{B}$). In the case of a ligand, that only binds to the receptor, that condition reads:

$$\mathrm{P_L} = \tilde{\mathrm{D}}_{\mathrm{L}}\,[\mathrm{L}] + \tilde{\mathrm{D}}_{\mathrm{L-R}}\,[\mathrm{L-R}] \tag{9}$$

The degradation rates are usually assumed as constants but the production rates are modelled in a more complex way. For instance, the production rate of ligand L can be split into a term corresponding to endogenous production, $\mathrm{P_{L,b}}$, and a term accounting for external dosage, $\mathrm{P_{L,d}}$:

$$\mathrm{P_L} = \mathrm{P_{L,b}} + \mathrm{P_{L,d}} \tag{10}$$

The endogenous production is sometimes modelled by the following equation:

$$\mathrm{P_{L,b}} = \sum_{\mathrm{X,Y}} \beta_{\mathrm{L,Y}}\, \pi^{\mathrm{X}}_{\mathrm{act/rep,Y}}\, \mathrm{Y} \left(1 - \frac{[\mathrm{L}]}{[\mathrm{L}]_{\mathrm{max}}}\right) \tag{11}$$

where Y is the concentration of the cell type Y producing L with a production rate $\beta_{\mathrm{L,Y}}$, regulated by the species X through the activator or repressor

function $\pi^{X}_{act/rep,Y}$. The parenthesis establishes a saturation condition in such a way that ligand is not produced if its concentration reaches the maximum or saturation value, $[L]_{max}$.

As described by Pivonka et al. [3] the activation of a certain biological process regulated by the formation of the complex L–R is given by the ratio between the receptors R occupied by ligands L and the total number of receptors:

$$\pi^{L}_{act,Y} = \frac{[L-R]}{[R]_{tot}} = \frac{[L-R]}{[R] + \sum_{L'}[L'-R]} \tag{12}$$

Similarly, the repressor action of the binding is given by the complementary to one of the latter:

$$\pi^{L}_{rep,Y} = \frac{[R]_{tot} - [L-R]}{[R]_{tot}} = \frac{[R] + \sum_{L' \neq L}[L'-R]}{[R] + \sum_{L'}[L'-R]} \tag{13}$$

In case of a single ligand the latter expressions yield the first-order Hill activator and repressor functions:

$$\pi^{L}_{act,Y} = \frac{[L]}{[L] + K^{L-R}_{act,Y}} \tag{14}$$

$$\pi^{L}_{rep,Y} = \frac{K^{L-R}_{rep,Y}}{K^{L-R}_{rep,Y} + [L]} \tag{15}$$

3. Competitive RANK-RANKL-OPG binding

The RANK-RANKL-OPG signalling pathway controls the differentiation of uncommitted osteoclast progenitors and osteoclasts maturation, respectively through π^{RANKL}_{act,Oc_u} and π^{RANKL}_{act,Oc_p} (see Eq. 7 in the main document). Thus, an imbalance in that pathway, such as that occurring after menopause, may result in the development of osteoporosis. Following Martin et al. [1], the concentrations of OPG, RANK and RANKL are given by the following equations:

$$[\mathrm{OPG}] = \frac{\mathrm{P_{OPG}}}{\tilde{\mathrm{D}}_{\mathrm{OPG}} + \frac{\tilde{\mathrm{D}}_{\mathrm{OPG-RANKL}}\,[\mathrm{RANKL}]}{\mathrm{K_{OPG-RANKL}}}} \tag{16}$$

$$[\mathrm{RANK}] = \frac{\mathrm{N_{Oc_p}^{RANK}\,Oc_p}}{1 + \frac{[\mathrm{RANK}]}{\mathrm{K_{RANK-RANKL}}}} \tag{17}$$

$$\begin{aligned}[\mathrm{RANKL}] =& \mathrm{P_{RANKL}} \cdot \left[\tilde{\mathrm{D}}_{\mathrm{RANKL}} + \frac{\tilde{\mathrm{D}}_{\mathrm{OPG-RANKL}}}{\mathrm{K_{OPG-RANKL}}} \cdot [\mathrm{OPG}]\right. \\ &\left. + \frac{\tilde{\mathrm{D}}_{\mathrm{RANK-RANKL}}}{\mathrm{K_{RANK-RANKL}}} \cdot [\mathrm{RANK}]\right]^{-1}\end{aligned} \tag{18}$$

where $\tilde{\mathrm{D}}_{\mathrm{X}}$ and $\tilde{\mathrm{D}}_{\mathrm{X-Y}}$ are the degradation rates of the factor X and the complex X-Y, respectively; $\mathrm{K_{X-Y}}$ is the dissociation constant of the complex X-Y and $\mathrm{N_{Oc_p}^{RANK}}$ is the number of RANK receptors per osteoclast precursor. $\mathrm{P_{OPG}}$ is the production rate of OPG by active osteoblasts:

$$\mathrm{P_{OPG}} = \beta_{\mathrm{OPG,Ob_a}}\,\pi_{\mathrm{rep,Ob_a}}^{\mathrm{PTH}}\,\mathrm{Ob_a}\left(1 - \frac{[\mathrm{OPG}]}{[\mathrm{OPG_{max}}]}\right) \tag{19}$$

where $\beta_{\mathrm{OPG,Ob_a}}$ is the OPG production rate, $\pi_{\mathrm{rep,Ob_a}}^{\mathrm{PTH}}$ is the repressor function that quantifies the effect of PTH on the production of OPG and $[\mathrm{OPG_{max}}]$ is the saturation concentration of OPG above which no further production takes place. $\mathrm{P_{RANKL}}$ is the RANKL production rate of Eq. (18) and it is explained in the main document.

Finally, $[\mathrm{RANKL}]_{\mathrm{tot}}$ is the total concentration of RANKL (bound and free) and is defined as follows:

$$\begin{aligned}[\mathrm{RANKL}]_{\mathrm{tot}} =& [\mathrm{RANKL}]\cdot \\ &\left(1 + \frac{[\mathrm{OPG}]}{\mathrm{K_{OPG-RANKL}}} + \frac{[\mathrm{RANK}]}{\mathrm{K_{RANK-RANKL}}} + \frac{[\mathrm{Dmab}]_{\mathrm{BC}}}{\mathrm{K_{RANKL-Dmab}}}\right)\end{aligned} \tag{20}$$

4. Competitive binding Wnt–Scl–LRP5/6-Rmab

The previous equations can be used to describe the competitive binding Wnt–Scl–LRP5/6 and the sclerostin antibody: Rmab. Wnt signaling is an anabolic pathway promoting the proliferation of osteoblast precursors and hence bone formation. Extracellular Wnt binds to Frizzled and the lipoprotein receptor-related protein LRP5/6, so triggering intracellular activation of β-catenin. Sclerostin, produced by osteocytes, modulates the signaling pathway by its interaction with LRP5/6 receptors. This prevents the formation of the Wnt-Frizzled-LRP5/6 complex and therefore hinders preosteoblasts proliferation. Competitive Wnt–Scl–LRP5/6-Rmab binding is modelled as follows. First, Eq. (7) reads for LRP5/6:

$$[\mathrm{LRP5/6}]_{\mathrm{tot}} = [\mathrm{LRP5/6}] \cdot \left(1 + \frac{[\mathrm{Wnt}]}{\mathrm{K}_{\mathrm{Wnt-LRP5/6}}} + \frac{[\mathrm{Scl}]}{\mathrm{K}_{\mathrm{Scl-LRP5/6}}}\right) \tag{21}$$

The production of sclerostin is given by an equation like (9), which now reads:

$$\mathrm{P}_{\mathrm{Scl,b}} + \mathrm{P}_{\mathrm{Scl,d}} = \tilde{\mathrm{D}}_{\mathrm{Scl}}\,[\mathrm{Scl}] + \tilde{\mathrm{D}}_{\mathrm{Scl-LRP5/6}}\,[\mathrm{Scl-LRP5/6}] + \tilde{\mathrm{D}}_{\mathrm{Rmab-Scl}}\,[\mathrm{Rmab-Scl}] \tag{22}$$

where $\tilde{\mathrm{D}}_{\mathrm{Scl}}$, $\tilde{\mathrm{D}}_{\mathrm{Scl-LRP5/6}}$ and $\tilde{\mathrm{D}}_{\mathrm{Rmab-Scl}}$ are the degradation rates of sclerostin, the sclerostin-LRP5/6 complex and the sclerostin-Rmab complex, respectively. The concentration of these complex are given by the receptor-ligand binding equation (3a), which read here:

$$[\mathrm{Scl-LRP5/6}] = \frac{[\mathrm{Scl}]\,[\mathrm{LRP5/6}]}{\mathrm{K}_{\mathrm{Scl-LRP5/6}}} \tag{23}$$

$$[\mathrm{Rmab-Scl}] = \frac{[\mathrm{Scl}]\,[\mathrm{Rmab}]_{\mathrm{BC}}}{\mathrm{K}_{\mathrm{Rmab-Scl}}} \tag{24}$$

The external dosage of sclerostin, $\mathrm{P}_{\mathrm{Scl,d}}$, grows with age as seen in Ruiz-Lozano et al. [4] and the endogenous production of sclerostin by osteocytes is:

$$\mathrm{P_{Scl,b}} = \beta_{\mathrm{Scl,Ot}}\, \pi_{\mathrm{rep,Scl}}^{|\varepsilon|_{\max}}\, \mathrm{Ot}\, \left(1 - \frac{[\mathrm{Scl}]}{[\mathrm{Scl}]_{\max}}\right) \tag{25}$$

where $\beta_{\mathrm{Scl,Ot}}$ and $[\mathrm{Scl}]_{\max}$ are, respectively, the sclerostin production rate and its maximum concentration. The production of sclerostin by osteocytes is downregulated by the mechanical stimulus through the repressor function $\pi_{\mathrm{rep,Scl}}^{|\varepsilon|_{\max}}$ (see Eq. (36) later on).

Following Martin et al. [1] we assumed that the total number of LRP5/6 receptors per osteoblast precursor ($\mathrm{N_{OB_p}^{LRP5/6}}$) is constant and thus:

$$[\mathrm{LRP5/6}]_{\mathrm{tot}} = \mathrm{N_{OB_p}^{LRP5/6}}\, \mathrm{Ob_p} \tag{26}$$

Solving for [LRP5/6] in Eq. (21) and considering Eqs. (6) to obtain the expressions for the concentrations of [Scl] and $[\mathrm{Rmab}]_{\mathrm{BC}}$, we arrived at the following equations:

$$[\mathrm{LRP5/6}] = \frac{[\mathrm{LRP5/6}]_{\mathrm{tot}}}{1 + \frac{[\mathrm{Wnt}]}{\mathrm{K_{Wnt-LRP5/6}}} + \frac{[\mathrm{Scl}]}{\mathrm{K_{Scl-LRP5/6}}}} \tag{27a}$$

$$[\mathrm{Scl}] = \frac{\mathrm{P_{Scl}}}{\tilde{\mathrm{D}}_{\mathrm{Scl}} + \frac{\tilde{\mathrm{D}}_{\mathrm{Scl-LRP5/6}}}{\mathrm{K_{Scl-LRP5/6}}}\,[\mathrm{Scl}] + \frac{\tilde{\mathrm{D}}_{\mathrm{Rmab-Scl}}}{\mathrm{K_{Rmab-Scl}}}\,[\mathrm{Rmab}]_{\mathrm{BC}}} \tag{27b}$$

$$[\mathrm{Rmab}]_{\mathrm{BC}} = \frac{\mathrm{P_{Rmab_{BC}}}}{\tilde{\mathrm{D}}_{\mathrm{Rmab_{BC}}} + \frac{\tilde{\mathrm{D}}_{\mathrm{Rmab-Scl}}}{\mathrm{K_{Rmab-Scl}}}\,[\mathrm{Scl}]} \tag{27c}$$

Finally, using Eqs. (12) and (26), the activator function in the $\mathrm{Ob_p}$ proliferation term can be calculated as:

$$\pi_{\mathrm{act,Ob_p}}^{\mathrm{Wnt}} = \frac{[\mathrm{Wnt} - \mathrm{LRP5/6}]}{[\mathrm{LRP5/6}]_{\mathrm{tot}}} = \frac{[\mathrm{Wnt}]\,[\mathrm{LRP5/6}]}{\mathrm{K_{Wnt-LRP5/6}}\,[\mathrm{LRP5/6}]_{\mathrm{tot}}} \tag{28}$$

5. Co-regulation of RANKL via PTH and NO concentration

RANKL transcription is upregulated by parathyroid hormone (PTH) and downregulated by nitric oxide (NO). In the model developed by Martin et al.

[1] this antagonistic influence was merged into a co-regulatory function capturing both effects.

$$\pi^{\mathrm{PTH,NO}}_{\mathrm{act/rep,RANKL}} = \lambda_{\mathrm{s}} \left(\pi^{\mathrm{PTH}}_{\mathrm{act,RANKL}} + \pi^{\mathrm{NO}}_{\mathrm{rep,RANKL}} \right) + \lambda_{\mathrm{c}}\, \pi^{\mathrm{PTH}}_{\mathrm{act,RANKL}} \cdot \pi^{\mathrm{NO}}_{\mathrm{rep,RANKL}} \tag{29}$$

where the activator function accounting for the effect of PTH is:

$$\pi^{\mathrm{PTH}}_{\mathrm{act,RANKL}} = \frac{[\mathrm{PTH}]}{[\mathrm{PTH}] + \mathrm{K}^{\mathrm{PTH}}_{\mathrm{act}}} \tag{30}$$

and the repressor effect on OPG (see Eq. (19)) is accounted for through the function:

$$\pi^{\mathrm{PTH}}_{\mathrm{rep,Ob_a}} = \frac{\mathrm{K}^{\mathrm{PTH}}_{\mathrm{rep}}}{[\mathrm{PTH}] + \mathrm{K}^{\mathrm{PTH}}_{\mathrm{rep}}} \tag{31}$$

being $\mathrm{K}^{\mathrm{PTH}}_{\mathrm{act}}$ and $\mathrm{K}^{\mathrm{PTH}}_{\mathrm{rep}}$ constants and the concentration of PTH given by:

$$[\mathrm{PTH}] = \frac{\beta_{\mathrm{PTH}}}{\tilde{\mathrm{D}}_{\mathrm{PTH}}} \tag{32}$$

which comes from Eqs. (8) to (11) when there is no ligand for the species, the external dosage is null ($\mathrm{P}_{\mathrm{PTH,d}} = 0$), the endogenous production rate is not regulated ($\pi^{\mathrm{X}}_{\mathrm{act/rep,Y}} \cdot \mathrm{Y} = 1$ see Eq. (11)) and the saturation value $[\mathrm{PTH}]_{\mathrm{max}}$ is large enough to assume the parenthesis equal to 1. β_{PTH} and $\tilde{\mathrm{D}}_{\mathrm{PTH}}$ are the endogenous production and degradation rate of PTH, respectively. On the other hand, the factor corresponding to nitric oxide is:

$$\pi^{\mathrm{NO}}_{\mathrm{rep,RANKL}} = \frac{\mathrm{K}^{\mathrm{NO}}_{\mathrm{rep}}}{[\mathrm{NO}] + \mathrm{K}^{\mathrm{NO}}_{\mathrm{rep}}} \tag{33}$$

with $\mathrm{K}^{\mathrm{NO}}_{\mathrm{rep}}$ a constant and the concentration of NO given by:

$$[\mathrm{NO}] = \frac{\mathrm{P}_{\mathrm{NO,d}} + \beta_{\mathrm{NO,Ot}}\, \pi^{|\varepsilon|_{\mathrm{max}}}_{\mathrm{act,NO}}\, \mathrm{Ot}}{\tilde{\mathrm{D}}_{\mathrm{NO}} + \frac{\beta_{\mathrm{NO,Ot}}\, \pi^{|\varepsilon|_{\mathrm{max}}}_{\mathrm{act,NO}}\, \mathrm{Ot}}{[\mathrm{NO}]_{\mathrm{max}}}} \tag{34}$$

which also comes from Eq. (8) in the absence of ligands. The external dosage of nitric oxide $P_{NO,d}$ is set to zero in this study, $\beta_{NO,Ot}$, $\tilde{D}_{NO}$ and $[NO]_{max}$ are, respectively, the endogenous production and degradation rate of nitric oxide and its maximum content. The factor $\pi_{act,NO}^{|\varepsilon|_{max}}$ is the mechanical feedback activator function that accounts for the production of NO by osteocytes. This function and the repressor function affecting the production of sclerostin by osteocytes (see Eq. (25)) are defined by the following sigmoidal functions:

$$\pi_{act,NO}^{|\varepsilon|_{max}} = \rho_{act} + \frac{(\alpha_{act} - \rho_{act})\ |\varepsilon|_{max}}{\delta_{act}^{\gamma_{act}} + |\varepsilon|_{max}^{\gamma_{act}}} \tag{35}$$

$$\pi_{rep,Scl}^{|\varepsilon|_{max}} = \alpha_{rep} - \frac{(\alpha_{rep} - \rho_{rep})\ |\varepsilon|_{max}^{\gamma_{rep}}}{\delta_{rep}^{\gamma_{rep}} + |\varepsilon|_{max}^{\gamma_{rep}}} \tag{36}$$

where $\rho_{\sim}$ and $\alpha_{\sim}$ are, respectively, the minimum and maximum anticipated response, $\gamma^{\sim}$ is the sigmoidicity, influencing the steepness of the response, $\delta_{\sim}$ is the value of the stimulus producing the half-maximal response [5], and $|\varepsilon|_{max}$ is the maximun principal strain in absolute value.

6. Damage

Targeted bone remodelling theories hypothesise that one of the major functions of bone remodelling is to remove microcracks from bone matrix, so avoiding an excessive accumulation of the latter, which could result in macroscopic failure [6]. The accumulation of microcracks in a particular volume of material is addressed here using a Continuum Damage Mechanics approach [7]. This theory introduces a damage variable, d, which is linked to the density of microcracks in a volume of material and to the loss of stiffness through Eq. (37). This variable is such that $d \in [0, 1]$, with d=0 corresponding to an undamaged state and d=1 to a local fracture or failure situation:

$$\mathbf{C} = (1 - d)\,\mathbf{C}_0 \tag{37}$$

where $\mathbf{C}$ and $\mathbf{C}_0$ are, respectively, the stiffness tensors of damaged and undamaged bone [7]. In the isotropic damage theory, Eq. (37) can be rewritten in terms of the respective Young's moduli, E and E_0, as $E = (1 - d)\,E_0$ [8, 9] (see Eq. (16) in the main document).

A balance of microdamage is considered through the accumulation due to fatigue loading and the removal due to bone remodelling, as osteoclasts resorb the damaged tissue, while the osteoid deposited by osteoblasts is initially intact. The evolution law for damage can be expressed as:

$$\dot{d} = \dot{d}_A - \dot{d}_R \tag{38}$$

where $\dot{d}_A$ is the rate of damage accumulation by fatigue loading and $\dot{d}_R$ is the rate of damage removal by bone remodelling. The latter is assessed by assuming that damage is uniformly distributed throughout the representative volume element (RVE). So, the amount of repaired damage is proportional to the damage present in that volume and to the volume of tissue being resorbed, $\dot{V}_r$, through the fraction that this volume represents within the bone matrix volume:

$$\dot{d}_R = d\,\frac{\dot{V}_r}{V_{bm}} = d\,\frac{k_{res}\cdot Oc_a}{f_{bm}} \tag{39}$$

Damage accumulation is evaluated following the procedure described in [10, 11]. This procedure makes use of the results of the experimental fatigue tests performed by Pattin et al. [9], who provided the evolution of damage with the strain level and the number of cycles. This evolution was mathematically modelled by García-Aznar et al. [12] to yield the following differential equation under tensile stresses:

$$\dot{d}_a = \dot{N}\,\frac{C_1}{C_2\,\gamma_f}\,(1-d)^{1-\gamma_f}\,\varepsilon_{max}^{\delta_f}\,\exp(-C_2\,(1-d)^{\gamma_f}) \tag{40}$$

where $\dot{N}$ is the number of cycles applied per unit time and ε_{max} is the maximum principal strain expressed in $\mu\varepsilon$.[1] The rest of parameters and constants of the model are:

$$\begin{aligned} C_1 &= \frac{e^{C_2}-1}{K_f([Ca])}; & \delta_f &= 14.1; \\ \gamma_f &= -0.018(\varepsilon_{max}-4100)+12; & C_2 &= -20; \end{aligned} \tag{41}$$

[1] In the damage model proposed by Martínez-Reina et al. [11], cracks were assumed to grow normal to the maximum strain direction and only under tensile strains.

where $K_f([Ca])$ is a function of the mineral content which will be defined next. The experimental tests perfomed by Pattin et al. [9] included an estimation of fatigue life, N_f, which was related to the deformation by the following expression:

$$N_f = \frac{K_f}{\varepsilon_{max}^{\delta_f}} \tag{42}$$

where K_f was assumed constant and equal to $1.445 \cdot 10^{53}$ in tension. Martínez-Reina et al. [10] introduced a correction in K_f to consider the degradation of the fatigue properties with the increase in mineral content. A life $N_f = 10^7$ cycles was assigned to the fatigue limit, which is usually assumed to occur for a given fraction of the ultimate tensile strain, ε_u/β, where the parameter β depends on the type of material [13] and $\beta = 2$ was assumed for bone [10] with good results. So, K_f was obtained from Eq. (42) as:

$$K_f([Ca]) = 10^7 \left(\frac{\varepsilon_u([Ca])}{\beta} \right)^{\delta_f} \tag{43}$$

where the ultimate tensile strain depends on the calcium concentration of bone matrix, [Ca], as Currey [14] showed. The following regression was fitted in [10] from the experimental results presented by Currey [14]:

$$\log \varepsilon_u = 31.452 - 11.341 \log [Ca] \tag{44}$$

where ε_u is expressed in $\mu\varepsilon$ and the concentration [Ca] is expressed in mg of calcium per g of bone matrix. This concentration is directly related to the ash fraction, α, which will be defined in the next section. More precisely, the relation $[Ca] = 398.8\,\alpha$ was assumed, based on the molecular weigths of hydroxyapatite and type I collagen [10].

7. Upregulation of RANKL expressed by osteocytes due to microstructural damage

As proposed in [15] we have assumed that RANKL expression by osteocytes is upregulated by the presence of microstructural damage in the bone

matrix through the factor $\pi^{dam}_{act,RANKL}$, which is defined as a sigmoidal function of damage, d:

$$\pi^{dam}_{act,RANKL} = \rho_{dam} + (\alpha_{dam} - \rho_{dam})\,(1 + K_{dam})\,\frac{d}{K_{dam} + d} \tag{45}$$

where K_{dam} is a constant, ρ_{dam} is the minimum value of the factor $\pi^{dam}_{act,RANKL}$, corresponding to d=0, while α_{dam} is its maximum value, corresponding to d=1.

8. Two-Compartment PK Model of Denosumab

Following the pharmacokinetic model developed by Martínez-Reina et al. [16], a first-order rate process (k_{aD}) governs the absorption of the drug (Dose) from the subcutaneous (SC) injection site into the central compartment ($[Dmab]_{CC}$), being V_{cD}/F_D the volume of the central compartment adjusted for bioavailability. The drug elimination from the central compartment is described by a combination of a linear first-order process (k_{elD}) and a non-linear saturation process (V_{maxD}, K_{MD}):

$$\frac{d\,[Dmab]_{CC}}{dt} = \frac{Dose}{V_{cD}/F_D} k_{aD} e^{-k_{aD} t} - \left[k_{elD}\,[Dmab]_{CC} + \frac{V_{maxD}}{V_{cD}/F_D} \frac{[Dmab]_{CC}}{K_{MD} + [Dmab]_{CC}} \right] \tag{46}$$

In Eq. (46) Dose is given in ng per kg of body weight and then $[Dmab]_{CC}$ is calculated in ng/ml and subsequently converted into pmol/l, through the molecular weight of denosumab M_{Dmab} = 149 kDa.

In previous models (Martínez-Reina and Pivonka [17], Martínez-Reina et al. [18]) they have assumed that a fraction of the Dmab present in the central compartment was available in the bone compartment to compete with RANK to bind to RANKL. However, this availability actually implied a reversible exchange of Dmab between both compartments. Given the affinity of Dmab for RANKL, which is expressed by osteoblasts precursors within the bone compartment, a flux from the central compartment to the bone compartment seems more plausible than a reversible exchange. To this end, they added the bone compartment to the PK model in Martínez-Reina et al.

[16]. The term in square brackets in Eq. (46) represents the elimination from the central compartment in the model of Marathe et al. [19] We have assumed that only a fraction $(1-\zeta_{\mathrm{D}})$ of this term is actually eliminated via urine and the rest, ζ_{D}, is the flux of denosumab into the bone compartment. In turn, the latter fraction can be considered as $\mathrm{P}_{\mathrm{Dmab_{BC}}}$, the production term of denosumab in the competitive binding reactions between RANKL, OPG and Dmab:

$$\mathrm{P}_{\mathrm{Dmab_{BC}}} = \zeta_{\mathrm{D}} \left[\mathrm{k_{elD}} \left[\mathrm{Dmab}\right]_{\mathrm{CC}} + \frac{\mathrm{V_{maxD}}}{\mathrm{V_{cD}/F_D}} \frac{\left[\mathrm{Dmab}\right]_{\mathrm{CC}}}{\mathrm{K_{MD}} + \left[\mathrm{Dmab}\right]_{\mathrm{CC}}} \right] \tag{47}$$

This production rate can be replaced in the expression that gives the concentration of ligands in competitive binding reactions (See Section 2), ie:

$$\left[\mathrm{Dmab}\right]_{\mathrm{BC}} = \frac{\mathrm{P}_{\mathrm{Dmab_{BC}}}}{\tilde{\mathrm{D}}_{\mathrm{Dmab_{BC}}} + \frac{\tilde{\mathrm{D}}_{\mathrm{RANKL-Dmab}}}{\mathrm{K_{RANKL-Dmab}}} \cdot \left[\mathrm{RANKL}\right]} \tag{48}$$

9. Regulatory role of TGF-β

TGF–β is stored in the bone matrix and released during resorption by osteoclasts. Its concentration is calculated following Pivonka et al. [2]:

$$\left[\mathrm{TGF-\beta}\right] = \frac{\alpha_{\mathrm{TGF-\beta}}\ \mathrm{k_{res}}\ \mathrm{Oc_a}}{\tilde{\mathrm{D}}_{\mathrm{TGF-\beta}}} \tag{49}$$

where $\alpha_{\mathrm{TGF-\beta}}$ is the concentration of TGF–β in bone matrix and $\tilde{\mathrm{D}}_{\mathrm{TGF-\beta}}$ is the TGF–β degradation rate. The concentration of TGF–β is used to define the activator/repressor functions in Eqs. (1)-(4) of the main document. These functions control the upregulation of the differentiation of $\mathrm{Ob_u}$ into $\mathrm{Ob_p}$, the upregulation of osteoclast apoptosis and the downregulation of the differentiation of $\mathrm{Ob_p}$ into $\mathrm{Ob_a}$:

$$\pi^{\mathrm{TGF-\beta}}_{\mathrm{act,Ob_u}} = \pi^{\mathrm{TGF-\beta}}_{\mathrm{act,Oc_p}} = \frac{\left[\mathrm{TGF-\beta}\right]}{\mathrm{K}^{\mathrm{TGF-\beta}}_{\mathrm{act}} + \left[\mathrm{TGF-\beta}\right]} \tag{50}$$

$$\pi^{\mathrm{TGF-\beta}}_{\mathrm{rep,Ob_p}} = \frac{\mathrm{K}^{\mathrm{TGF-\beta}}_{\mathrm{rep}}}{\mathrm{K}^{\mathrm{TGF-\beta}}_{\mathrm{rep}} + \left[\mathrm{TGF-\beta}\right]} \tag{51}$$

with $\mathrm{K}^{\mathrm{TGF-\beta}}_{\mathrm{act}}$ and $\mathrm{K}^{\mathrm{TGF-\beta}}_{\mathrm{rep}}$ the activation and repression constants, respectively.

10. Proliferation of osteoblast precursors

Let us recall the differential equation of osteoblast precursors.

$$\begin{aligned}\frac{\mathrm{d}\,\mathrm{Ob_p}}{\mathrm{dt}} &= \mathrm{D_{Ob_u}} \cdot \mathrm{Ob_u} \cdot \pi^{\mathrm{TGF-\beta}}_{\mathrm{act,Ob_u}} - \mathrm{D_{Ob_p}} \cdot \mathrm{Ob_p} \cdot \pi^{\mathrm{TGF-\beta}}_{\mathrm{rep,Ob_p}} \\ &+ \mathrm{P_{Ob_p}} \cdot \mathrm{Ob_p} \cdot \pi^{\mathrm{Wnt}}_{\mathrm{act,Ob_p}}\end{aligned} \tag{52}$$

We can rewrite this equation as:

$$\frac{\mathrm{d}\,\mathrm{Ob_p}}{\mathrm{dt}} = \mathcal{D}_{\mathrm{Ob_u}} \cdot \mathrm{Ob_u} - \mathcal{D}_{\mathrm{Ob_p}} \cdot \mathrm{Ob_p} + \mathcal{P}_{\mathrm{Ob_p}} \cdot \mathrm{Ob_p} \tag{53}$$

where the terms in the right-hand side correspond, respectively, to the differentiation of $\mathrm{Ob_u}$ into $\mathrm{Ob_p}$, the differentiation of $\mathrm{Ob_p}$ into $\mathrm{Ob_a}$ and the proliferation of $\mathrm{Ob_p}$ at a rate $\mathcal{P}_{\mathrm{Ob_p}}$ which is determined by $\mathrm{P_{Ob_p}}$ and the Wnt–Scl–LRP5/6 signalling pathway through $\pi^{\mathrm{Wnt}}_{\mathrm{act,Ob_p}}$ (see Eq. (52)). As discussed in Buenzli et al. [20], a necessary condition for the $\mathrm{Ob_p}$ population to stay bounded and to converge to a meaningful steady-state (with finite, positive cell densities) is that:

$$\mathcal{P}_{\mathrm{Ob_p}} - \mathcal{D}_{\mathrm{Ob_p}} < 0 \quad \text{as} \quad \mathrm{t} \longrightarrow \infty \tag{54}$$

Following Buenzli et al. [20] $\mathrm{P_{Ob_p}}$ was defined considering a saturation factor:

$$\mathrm{P_{Ob_p}} = \begin{cases} \mathrm{P^0_{Ob_p}} \left(1 - \dfrac{\mathrm{Ob_p}}{\mathrm{Ob_p^{sat}}}\right) & \text{if} \quad \mathrm{Ob_p} < \mathrm{Ob_p^{sat}} \\ 0 & \text{if} \quad \mathrm{Ob_p} \geq \mathrm{Ob_p^{sat}} \end{cases} \tag{55}$$

where $\mathrm{P^0_{Ob_p}}$ is a constant and $\mathrm{Ob_p^{sat}}$ is the maximum concentration of osteoblast precursors above which no proliferation occurs. This saturation and the choice of $\mathrm{P^0_{Ob_p}}$ (see Table 1) ensures that Eq. (54) is fulfilled.

11. Algorithm of bone mineralisation

Bone tissue is made up of bone matrix and pores. Thus, the representative volume element, V_{RVE}, can be divided into the bone matrix volume, V_{bm}, and the volume of vascular pores, V_{vas}. In turn, bone matrix volume is divided into inorganic (mineral), organic (mainly collagen) and water phases, respectively designated as V_m, V_o and V_w:

$$V_{RVE} = V_{bm} + V_{vas} = V_m + V_o + V_w + V_{vas} \tag{56}$$

The volume fractions of extravascular bone matrix and vascular pores are respectively given by $f_{bm} = V_{bm}/V_{RVE}$ and $f_{vas} = 1 - f_{bm} = V_{vas}/V_{RVE}$. The mineral content is usually measured by the so-called ash fraction, the ratio between mass of mineral m_m (or ash mass) and dry mass (the sum of inorganic and organic mass):

$$\alpha = \frac{m_m}{m_m + m_o} = \frac{\rho_m V_m}{\rho_m V_m + \rho_o V_o} \tag{57}$$

where density of hydroxyapatite is taken for $\rho_m = 3.2\,\mathrm{g/cm^3}$ [14]. Organic phase is mainly composed of type I collagen, but other non-collagenous proteins are also present. Thus, $\rho_o = 1.41\,\mathrm{g/cm^3}$ was adjusted to provide a tissue density $\rho_t = 2.1\,\mathrm{g/cm^3}$ for the completely mineralised tissue $\alpha = 0.73$ [12].

Specific volumes are defined by: $v_o = V_o/V_{bm}$, $v_m = V_m/V_{bm}$ and $v_w = V_w/V_{bm}$, which implies that $v_o + v_w + v_m = 1$. Then, Eq.(57) can be given in terms of the specific volumes:

$$\alpha = \frac{\rho_m v_m}{\rho_m v_m + \rho_o v_o} \tag{58}$$

Bone tissue density is given by:

$$\rho_t = \frac{m}{V_{bm}} = \rho_m v_m + \rho_o v_o + \rho_w v_w \tag{59}$$

Mineral accumulates by displacing water present in bone matrix [21]. Therefore, the volume ratio of organic phase is assumed constant during the mineralisation process, $v_o = 3/7$ [22]; while the variations of mineral and water volume ratios hold $\Delta v_m = -\Delta v_w$. We have followed Hernández et al. [21] to assess the increase of v_m with time, by distinguishing the mineralisation lag time; the primary phase, with a linear increase, and the secondary phase, with an exponentially decreasing rate:

$$v_m(t) = \begin{cases} 0 & \text{if} \quad t \leq t_{mlt} \\ v_{m\,prim}\,\dfrac{t - t_{mlt}}{t_{prim}} & \text{if} \quad t_{mlt} < t \leq t_{prim} + t_{mlt} \\ v_{m\,max} - (v_{m\,max} - v_{m\,prim})\,e^{-\kappa\cdot(t - t_{prim} - t_{mlt})} & \text{if} \quad t_{prim} + t_{mlt} < t \end{cases} \tag{60}$$

where t_{mlt} and t_{prim} are, respectively, the length of the mineralisation lag time and the primary phase; $v_{m\,prim}$ is the mineral specific volume at the end of the primary phase, corresponding to $\alpha = 0.45$ [21]; $v_{m\,max}$ is the mineral specific volume corresponding to the maximum calcium content, 300 mg/g [14]; and κ is a parameter measuring the rate of mineral deposition during the secondary phase. Note that, with the assumptions made above, Eqs. (58) and (59) establish a biunivocal relation between α and ρ_t.

The amount of mineral contained in a RVE depends on the age of the tissue through Eq. (60), but the RVE can be made up of tissue patches formed in the recent history, viz. of different ages. Moreover, the tissue within the RVE can be resorbed, which puts the mineral back into the blood flow. The amounts of tissue of different ages contained in the RVE are estimated using the algorithm depicted in Fig. 1 [11]. $\overline{V}_{form}(t, \tau)$ provides the bone volume formed τ days ago and still present (not yet resorbed) at time t. Knowing the distribution of tissue patches of different ages at day t (left column) and the volume formed ($V_{form}(t) = k_{form}\,Ob_a(t)$) and resorbed that day ($V_{res}(t) = k_{res}\,Oc_a(t)$), the distribution at day t+1 (right column) can be estimated:

$$\overline{V}_{form}(t+1, i+1) = \overline{V}_{form}(t, i) - V_{res}(t)\,\frac{\overline{V}_{form}(t, i)}{V_b(t)} \tag{61}$$

Finally, the mineral content of each patch is summed to estimate the average mineral content of the RVE at day t+1.

$$v_m(t+1) = \frac{\sum_{i=0}^{t_R} \overline{V}_{form}(t+1, i) \cdot v_m(i)}{V_b(t+1)} \tag{62}$$

where the mineral contents of the patches, $v_m(i)$, are calculated through Eq. (60). t_R represents the residence time, e.g. the typical time the patch tissue remains within the bone before being resorbed. This residence time can be very large but the queue can be truncated at a shorter time to reduce the computational cost. See [23] for more details.

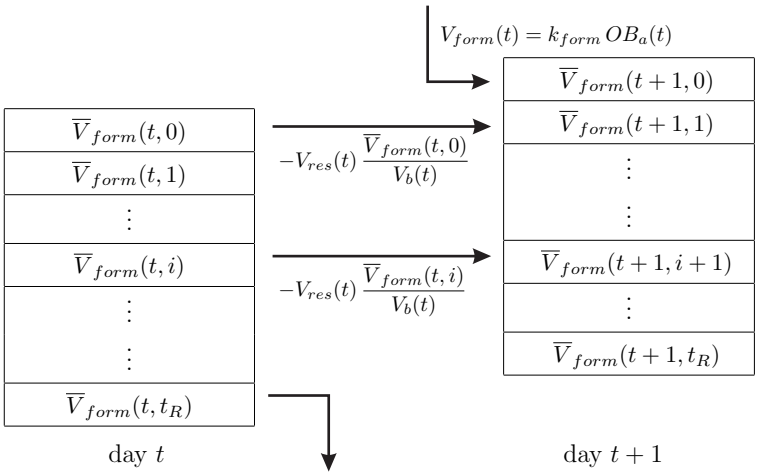

Figure 1: FIFO (first in - first out) queue algorithm used to update the distribution of tissue patches of different ages within the RVE.

It must be noted here that the recursive character of this mineralisation algorithm makes it necessary to integrate the set of differential equations that governs the model using an explicit integration scheme.

12. Model constants

The model constants, except for those related to the damage and mineralisation algorithms, which were given in the main document, are provided in the following table.

Constant	Value	Units
Cell constants: differentiation, proliferation, apoptosis, activity		
Ob_u	0.01	pM
Oc_u	0.01	pM
D_{Ob_u}	0.01	day^{-1}
D_{Ob_p}	0.0705	day^{-1}
$P^0_{Ob_p}$	3.47	day^{-1}
Ob_p^{sat}	0.005	pM
D_{Oc_u}	0.0388	day^{-1}
D_{Oc_p}	0.1216	day^{-1}
Δ_{Ob_a}	0.3502	day^{-1}
A_{Oc_a}	4.5	day^{-1}
η	$4.143 \cdot 10^{-4}$	pM / %[2]
k_{res}	200	% day^{-1} pM^{-1}
k_{form}	40	% day^{-1} pM^{-1}
RANK-RANKL-OPG signalling pathway		
$\tilde{D}_{OPG}$	0.35	day^{-1}
$\tilde{D}_{RANKL}$	0.4053	day^{-1}
$\tilde{D}_{Dmab_{BC}}$	16.22 *	day^{-1}
$\tilde{D}_{OPG-RANKL}$	559.67	day^{-1}
$\tilde{D}_{RANK-RANKL}$	10.132	day^{-1}
$\tilde{D}_{Dmab-RANKL}$	10.132 *	day^{-1}
$K_{OPG-RANKL}$	2300	pM
$K_{RANK-RANKL}$	10	pM

Continued on next page

[2]Recall that f_{bm} is expressed in %.

Constant	Value	Units
$K_{Dmab-RANKL}$	9.2	pM
$N_{Oc_p}^{RANK}$	$4.16 \cdot 10^3$	pM RANK / pM cell
β_{OPG,Ob_a}	$1.3 \cdot 10^5$ *	pM OPG / pM cell day^{-1}
$[OPG]_{max}$	$1.314 \cdot 10^2$	pM
$[RANKL]_{max}$	41.584	pM
$\beta_{RANKL,Ot}$	$2.836 \cdot 10^3$	pM RANKL / pM cell day^{-1}
β_{RANKL,Ob_p}	$2.14 \cdot 10^2$	pM RANKL / pM cell day^{-1}
K_{act,Oc_u}^{RANKL}	7.487	pM
K_{act,Oc_p}^{RANKL}	1.497	pM
Upregulation of RANKL via damage		
ρ_{dam}	0.04 *	-
α_{dam}	1 *	-
K_{dam}	0.28 *	-
Competitive binding Wnt-Scl-LRP5/6		
$\tilde{D}_{Scl}^0$	5	day^{-1}
$\tilde{D}_{Scl-LRP5/6}$	50	day^{-1}
$K_{Wnt-LRP5/6}$	$1.079 \cdot 10^3$	pM
$K_{Scl-LRP5/6}$	8.57	pM
$N_{OB_p}^{LRP5/6}$	5	pM LRP5/6 / pM cell
$\beta_{Scl,Ot}$	$5 \cdot 10^4$ *	pM Scl / pM cell day^{-1}
[Wnt]	170	pM
$[Scl]_{max}$	70	pM
$P_{Scl,d}^0$	0	pM day^{-1}
Co-regulation of RANKL via PTH and NO		
λ_s	0.45	-
λ_c	74.66	-
K_{act}^{PTH}	0.65	pM
K_{rep}^{PTH}	0.223	pM
K_{rep}^{NO}	$5.24 \cdot 10^2$ *	pM
$[NO]_{max}$	$2 \cdot 10^8$	pM

Continued on next page

Constant	Value	Units
β_{PTH}	250	pM day $^{-1}$
$\tilde{D}_{PTH}$	83	day^{-1}
$\beta_{NO,Ot}$	$1.39 \cdot 10^{3}$ *	pM NO / pM cell day^{-1}
$\tilde{D}_{NO}$	$2.1 \cdot 10^{-3}$	day^{-1}
$P_{NO,d}$	0	pM day^{-1}
Dmab PK-PD constants *		
k_{aD}	0.17	day^{-1}
k_{elD}	$1.15 \cdot 10^{-2}$	day^{-1}
V_{cD}	77.9	ml kg^{-1}
F_D	1	-
K_{MD}	411	ng ml^{-1}
V_{maxD}	2672	ng kg^{-1} day^{-1}
ζ_D	0.4889	-
Rmab PK-PD constants *		
k_{aR}	0.2	day^{-1}
k_{elR}	0.1	day^{-1}
V_{cR}	80.9	ml kg^{-1}
F_R	1	-
K_{MR}	3000	ng ml^{-1}
V_{maxR}	$5 \cdot 10^{5}$	ng kg^{-1} day^{-1}
ζ_R	0.56	-
$\tilde{D}_{Rmab_{BC}}$	$1.18 \cdot 10^{-2}$	day^{-1}
PMO related constants *		
k_1	$2.3 \cdot 10^{-3}$	pM RANKL/pM Cell $days^{-2}$
k_2	$2.58 \cdot 10^{-5}$	pM RANKL/pM Cell $days^{-2}$
T^*	185	days
TGF-β related constants		
$\frac{\alpha_{TGF-\beta}\, k_{res}}{\tilde{D}_{TGF-\beta}}$	1	-
$K_{act}^{TGF-\beta}$	$5.633 \cdot 10^{-4}$	pM

Continued on next page

Constant	Value	Units
$K_{rep}^{TGF-\beta}$	$1.754 \cdot 10^{-4}$	pM
Parameters of mechanical regulation		
α_{rep}	1	-
α_{act}	1	-
ρ_{rep}	0	-
ρ_{act}	0	-
δ_{rep}	$1.3 \cdot 10^{-3}$ *	MPa
δ_{act}	$6.2 \cdot 10^{-4}$ *	MPa
γ_{rep}	6 *	-
γ_{act}	11.5 *	-
δ_{eq}	0.95	-
Mineralisation model *		
t_{mlt}	8	days
t_{prim}	14	days
$v_{m\,prim}$	0.12	-
$v_{m\,max}$	0.442	-
κ	0.01	-

Table 1: Values taken for the constants of the PK-PD model. All the constants were taken from the model developed by Martin et al. [1], except those marked with an asterisk.

All the constants in Table 1 were taken from the model developed by Martin et al. [1], except those marked with an asterisk. These changes were motivated by the fact that Martin et al. did not considered damage and the variable mineral content of bone matrix. Hence, those constants needed to be readjusted to reproduce the behaviour of the previous model. So, $\beta_{Scl,Ot}$ and $\beta_{NO,Ot}$ were readjusted to achieve the same sclerostin and NO levels. The constants of the block "Upregulation of RANKL via damage" are new since damage were not considered in the previous model. Their values were fitted as in [15], so that the contribution of damage to RANKL production is similar in normal situations (homeostasis) to the production of RANKL by osteoblast precursors. The constants of the block "Dmab PK-PD constants" are specific of the Dmab PK model and are taken from previous works [15, 18]. The constants of the block "Rmab PK-PD constants" are specific of the Rmab

PK model and were adjusted as explained in section 2 of the main document. The constants of the block "PMO related constants" were readjusted as done in [4], i.e. to reproduce the results of the longitudinal experimental study of Riggs et al. [24] on the evolution of the bone mineral density (BMD) in the vertebral spine of post-menopausal women. Martin et al. [1] did not account for variations in mineral content and assumed the bone matrix fraction to evolve in the same way as the BMD. Now that this limitation has been overcome by including the mineral content, it was necessary to readjust the constants.

References

[1] M. Martin, V. Sansalone, D. M. L. Cooper, et al. Mechanobiological osteocyte feedback drives mechanostat regulation of bone in a multiscale computational model. Biomechanics and Modeling in Mechanobiology 2019;18:1475–96. doi:10.1007/s10237-019-01158-w.

[2] P. Pivonka, J. Zimak, D.W. Smith, et al. Model structure and control of bone remodeling: A theoretical study. Bone 2008;43(2):249–63.

[3] P. Pivonka, P. Buenzli, C.R. Dunstan. A Systems Approach to Understanding Bone Cell Interactions in Health and Disease. USA: InTech. ISBN 9789535107927; 2012, p. 169–204.

[4] R. Ruiz-Lozano, J. L. Calvo-Gallego, P. Pivonka, M. McDonald, J. Martínez-Reina. An in-silico approach to elucidate the pathways leading to primary osteoporosis: age-related vs. postmenopausal. Biomech Model Mechanbiol 2024;doi:10.21203/rs.3.rs-3432139/v1.

[5] M.C. Peterson, M.M. Riggs. A physiologically based mathematical model of integrated calcium homeostasis and bone remodeling. Bone 2010;46(1):49–63.

[6] A. Parfitt. Targeted and nontargeted bone remodeling: relationship to basic multicellular unit origination and progression. Bone 2002;30(1):5–7.

[7] J. Lemaitre, J. Chaboche. Mechanics of Solid Materials. Cambridge, UK: Cambridge University Press; 1990,.

[8] P. Zioupos, J. Currey. Changes in the stiffness, strength, and toughness of human cortical bone with age. Bone 1998;22(1):57–66.

[9] C. Pattin, W. Caler, D. Carter. Cyclic mechanical property degradation during fatigue loading of cortical bone. Journal of Biomechanics 1996;29(1):69–79.

[10] J. Martínez-Reina, J.M. García-Aznar, J. Domínguez, M. Doblaré. On the role of bone damage in calcium homeostasis. J Theor Biol 2008;254(3):704–12.

[11] J. Martínez-Reina, J. García-Aznar, J. Domínguez, et al. A bone remodelling model including the directional activity of bmus. Biomechanics and Modelling in Mechanobiology 2009;8(2):111–27.

[12] J. García-Aznar, T. Rueberg, M. Doblaré. A bone remodelling model coupling microdamage growth and repair by 3d bmu-activity. Biomechanics and Modelling in Mechanobiology 2005;4(2-3):147–67. doi:10.1007/s10237-005-0067-x.

[13] R. Juvinall. Engineering Considerations of Stress, Strain and Strength. New York, USA: McGraw-Hill; 1967,.

[14] J. Currey. Tensile yield in compact bone is determined by strain, postyield behaviour by mineral content. J Biomech 2004;37(4):549–56. doi:10.1016/j.jbiomech.2003.08.008.

[15] J. Martínez-Reina, J.L. Calvo-Gallego, P. Pivonka. Combined effects of exercise and denosumab treatment on local failure in post-menopausal osteoporosis — insights from bone remodelling simulations accounting for mineralisation and damage. Front Bioeng Biotechnol 2021;9:635056. doi:10.3389/fbioe.2021.635056.

[16] J. Martínez-Reina, J. L. Calvo-Gallego, M. Martin, P. Pivonka. Assessment of strategies for safe drug discontinuation and transition of denosumab treatment in PMO – Insights from a mechanistic PK/PD model of bone turnover. Front Bioeng Biotechnol 2022;10:886579. doi:10.3389/fbioe.2022.886579.

[17] J. Martínez-Reina, P. Pivonka. Effects of long-term treatment of denosumab on bone mineral density: insights from an in-silico model of bone

mineralization. Bone 2019;125:87–95. doi:10.1016/j.bone.2019.04.022.

[18] J. Martínez-Reina, J. L. Calvo-Gallego, P. Pivonka. Are drug holidays a safe option in treatment of osteoporosis? – Insights from an in silico mechanistic PK–PD model of denosumab treatment of postmenopausal osteoporosis. J Mech Behav Biomed 2021;113:104140. doi:10.1016/j.jmbbm.2020.104140.

[19] D. D. Marathe, A. Marathe, D. E. Mager. Integrated model for denosumab and ibandronate pharmacodynamics in postmenopausal women. Biopharm Drug Dispos 2011;32(8):471–81. doi:10.1002/bdd.770.

[20] P. R. Buenzli, P. Pivonka, B. S. Gardiner, D. W. Smith. Modelling the anabolic response of bone using a cell population model. J Theor Biol 2012;307:42–52. doi:10.1016/j.jtbi.2012.04.019.

[21] C. J. Hernández, G. S. Beaupré, D. R. Carter. A model of mechanobiologic and metabolic influences on bone adaptation. J Rehabil Res Dev 2001;37(2):235–44.

[22] R. Martin. Porosity and specific surface of bone. Critical Reviews in Biomedical Engineering 1984;10(3):179–222.

[23] J. Martínez-Reina, P. Pivonka. Effects of long-term treatment of denosumab on bone mineral density: insights from an in-silico model of bone mineralization. Bone 2019;125:87–95. doi:10.1016/j.bone.2019.04.022.

[24] B.L. Riggs, J.L. Melton (III), R.A. Robb, J.J. Camp, E.J. Atkinson, J.M. Peterson, et al. Population-based study of age and sex differences in bone volumetric density, size, geometry, and structure at different skeletal sites . J Bone Miner Res 2004;19(12):1945–54. doi:10.1359/JBMR.040916.